

Code: 203.113.108  
Date: November 1, 1956

# RESEARCH PAPER

## A HIGH-RESOLUTION PERPENDICULAR MAGNETIC RECORDING HEAD

By

J. J. Hagopian  
F. B. Wood

November 1, 1956

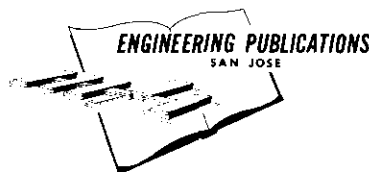
### ABSTRACT

Design and development of a low-cost, high-resolution magnetic recording element incorporating a gliding head structure is described. Test data is given showing reliable operation up to 40 tracks and 250 bits per inch. Theoretical analysis of the parameters involved in this system of recording is included in the Appendix. This report covers work done prior to January 1956.

### COMPANY CONFIDENTIAL

This document contains information of a proprietary nature. ALL INFORMATION CONTAINED HEREIN SHALL BE KEPT IN CONFIDENCE. No information shall be divulged to persons other than IBM employees authorized by the nature of their duties to receive such information, or individuals or organizations who are

authorized in writing by the Department of Engineering or its appointee to receive such information. Initial distribution limited to WHQ executives, managers of laboratories, assistant managers of laboratories, and other engineering management personnel. Further distribution must be cleared through these people.



INTERNATIONAL BUSINESS MACHINES CORPORATION  
RESEARCH LABORATORY, SAN JOSE, CALIFORNIA

## Introduction

Development of the magnetic recording head described in this report was undertaken primarily as a result of specifications ( 1, 2 ) given for an advanced design random access memory (RAM) employing magnetic discs. Requirements particularly bearing upon magnetic head design were:

1. Reduce maximum access time from 600 to 50 - milliseconds.
2. Increase record capacity from 5 to 50 - million characters.
3. Keep machine cost within that of present RAM.

These requirements were best satisfied by providing a cheap magnetic head for each disc face so as to reduce the time consumed in disc-to-disc transfer of a single head. In spite of cost limitations, satisfactory operation of the head was required under the following design refinements:

1. Bit density increased from 100 - to - 250 per in.
2. Track density increased from 20 - to - 40 per in.
3. Number of discs in file to be increased from 50 to 100, which placed a height limit of 0.1 in. on the head to be developed.

## Perpendicular vs. Longitudinal Recording

The complexity of fabricating "longitudinal" recording heads led to a consideration of "perpendicular" designs for the application at hand. Structural differences of the two forms can readily be understood from an examination of Fig. 1 which shows the basic Delta head now used on the present RAM, and the shielded probe recording head. The latter shows the present status in the perpendicular head design. Enlarged views of the pole-tip regions in planes parallel to the recorded tracks, and the principal directions of the magnetic flux at the pole-tips during recording, are shown in the lower part of Fig. 1, to illustrate the difference between the two modes of recording. Bixby<sup>3</sup> has mapped the field of the Delta head and has shown that the principal component in the recording medium is longitudinal with respect to the surface.

For the probe head, the principal component in the recording medium is seen to be perpendicular. A detailed flux plot together with a summary of the supporting calculations are given in Appendix A. These are shown in Figs. 8 and 11.

In the case of the Delta head, the recording disc base material is non-magnetic; RAM discs are of aluminum. As the probe head requires the disc base to be magnetically "soft", a mild steel has been used. High permeability materials plated or dispersion-painted on a non-magnetic base in a layer approximately 0.001 in. thick prior to coating with  $Fe_2O_3$  were also tried and found to offer promise as a practical disk construction.

### Advantages of Perpendicular Recording

Two features of the probe head constitute its chief advantages: the extreme simplicity of construction as shown in Fig. 1B, and the compatibility of the probe form with the gliding-head holder. Primarily because nearly one hp of air compressor capacity is required by a normal airhead, gliding support is necessary when an individual head for each disc face is used. The low cost element makes it feasible to employ such a ganged array of heads.

The working face of a simple gliding head must be lapped flat. Such a final operation on an integral-longitudinal element and holder assembly would radically modify the recording gap. Within limits, this is not the case for the shielded-probe head.

Read signal "overshoots" can be eliminated in the Delta head only by a rounding-off of the gap-tip corners, which is a delicate operation. An advantage of the perpendicular head is that overshoots may be eliminated with relative ease by exactly centering the probe in the shield gap.

The height of the longitudinal head cannot be greatly reduced without adding materially to fabrication difficulties. The height of the perpendicular head can be reduced with fewer complications -- a factor which permits reduction of the space between the discs, keeping the volume of the new file roughly within that of the old.

### Development of the Perpendicular Recording Head

Perpendicular recording heads initially constructed were not shielded, but consisted of a simple probe alone of the form shown in Fig. 1B. The read signal of such a head resulting from a single step change in recording current at saturation level is shown in Fig. 2A. In terms of recording surface dimensions, a bit recorded with this head spreads about 0.018 in. along a track at 20% of peak reading signal. This spreading is caused primarily by a rather wide "viewing angle" during reading, and to a lesser degree by a broad field distribution during recording. Eddy currents in the probe have a negligible effect on spreading as was demonstrated by testing a ferrite core with a 0.002 in. probe. The read signal for the ferrite head is shown in Fig. 2B.

A significant improvement in resolution is provided by the shield faces spaced by 0.001 in. brass or Mylar shims from the sides of the probe as shown in Fig. 1B. The shield faces are 0.002 in. permalloy or mu-metal with a silver plating 0.002 in. thick. While a degree of eddy current shielding is obtained from the silver film on the inside face, plating of the outside face has no important effect on performance, and is worn off in the final lapping operation on the head faces. Shield faces of .004" mu-metal, without silver plating have also been employed and equivalent results obtained. Fig. 2C shows the reading signal from the shielded probe head and indicates a major improvement in resolution. A theoretical calculation of the read signal is given in Appendix B.

Read Signal amplitude is not significantly affected by the probe shields, as shown by Fig. 2, indicating that there is little change in magnetic circuit reluctance involving the probe with, or without, the shields. Calculations presented in Appendix C verify this, and also show that the lack of a complete magnetic path for the head core results in less than 5% increase in reluctance.

### Performance of the Shielded Probe Head

In all of the tests now described, record current was supplied to one half of the head winding following D. C. erasure by current through the other half. The read signal was taken across the entire winding. The recording surface was initially erased by a 60 cps electromagnet. A "mild" steel disc was used with a 0.0007 in. red oxide recording surface, and surface speed was 670 in. per second. It is estimated that with the gliding element employed, the head-to-surface spacing was approximately .0005 in.

Fig. 3, 4, 5, and 6 show test results for head No. 62 and indicate that the specifications were adequately met. Fig. 3A shows the read signal after recording with various step-change magnitudes of current. For each test point, the recording head was first supplied with erase current of a magnitude equal to the recording current.

From Fig. 3B it is apparent that the saturation involved is that of the recording surface and not of the probe since read signal spread is not markedly increased at higher recording currents.

Fig. 4 presents the read signal after recording the NRZI pattern 1100100111 at 100-, 200-, and 275- bits per inch.

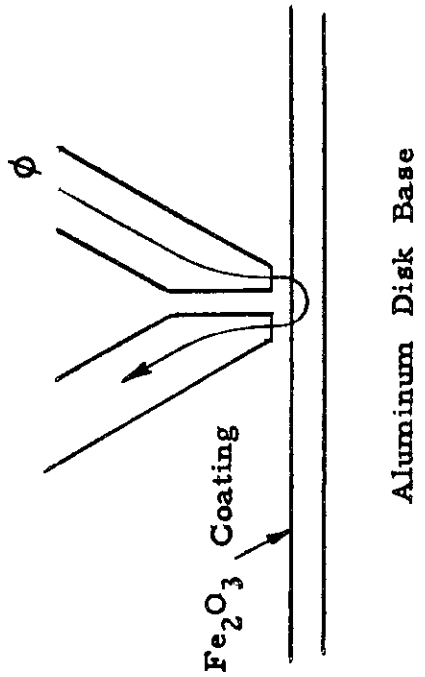
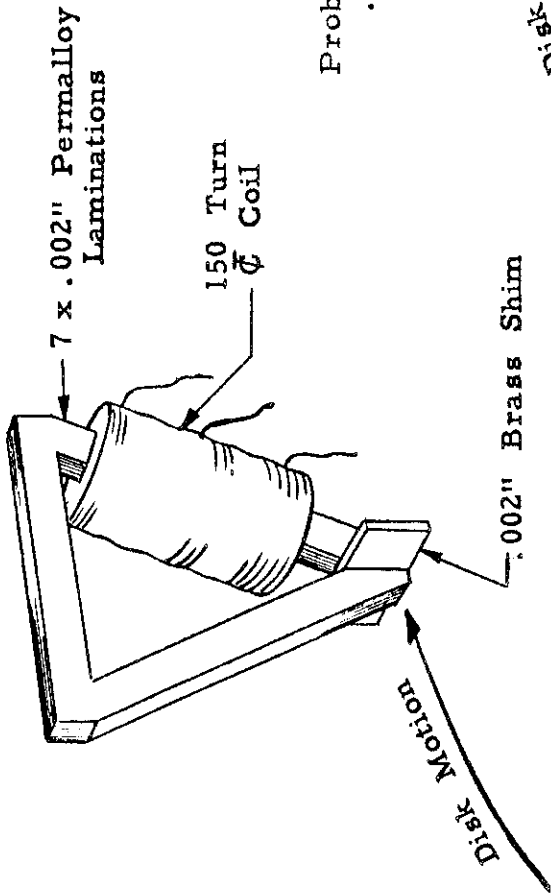
Track density performance is shown in Fig. 5. Unlike NRZI characters at 250 bits per inch were recorded on tracks 0.025 in. apart. The on-track read signals for each are shown in Fig. 5A. The read signals resulting from displacement of the head 0.010 in. to either side of the central track are shown in Fig. 5B, indicating excessive crosstalk.

Since it is anticipated that track selection will be accomplished by rotating a ganged array of these heads, head No. 62 was also tested for the effect of rotation on read amplitude and spread. The results plotted in Fig. 6 show that degradation of read signal does not occur until an angle of 30° is exceeded. This test was also conducted at 250 bits per inch.

### References

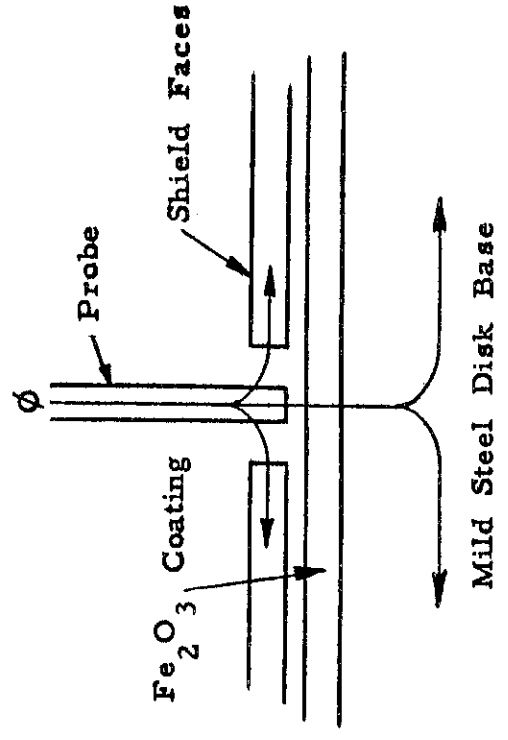
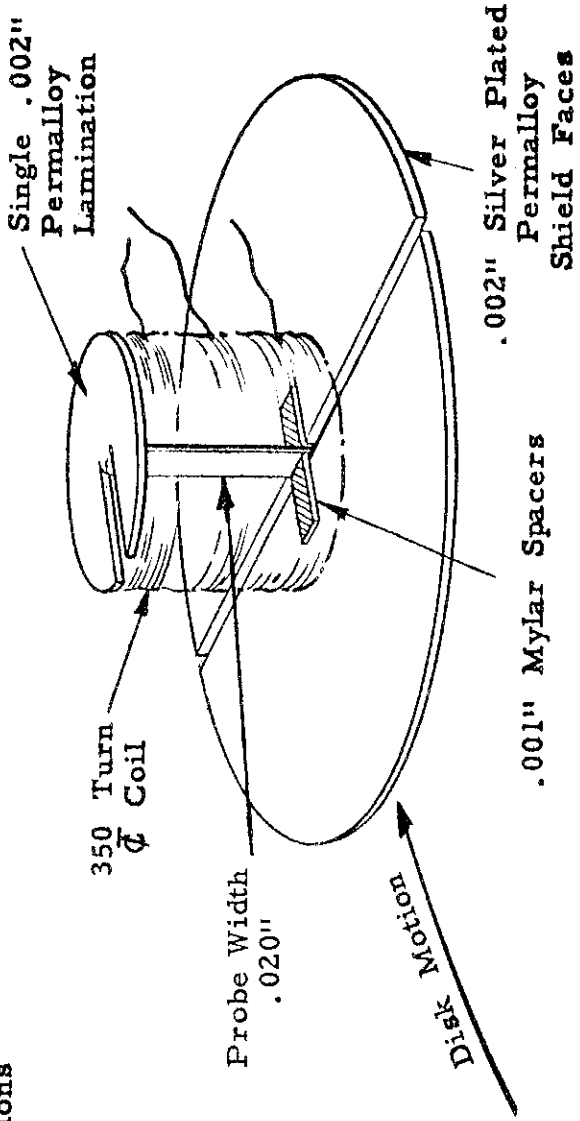
- (1) "High Speed Random Access File", Technical Record dated 10-15-54, J. J. Hagopian.
- (2) "Proposed Program for Development of a High-Performance Magnetic Disc Random Access Memory", Memo to R. B. Johnson, dated 2-11-55
- (3) "Investigations of Magnetic Recording", Internal report dated 6-30-54, L. H. Dixby, Jr.

DELTA HEAD  
LONGITUDINAL RECORDING



1A

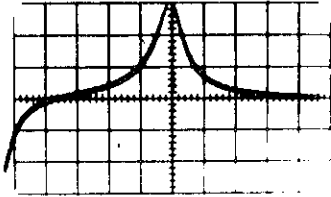
SHIELDED PROBE HEAD  
PERPENDICULAR RECORDING



1B

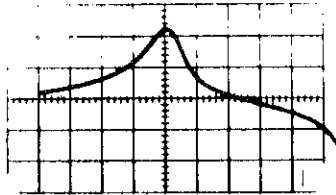
FIGURE 1

Figure 2A



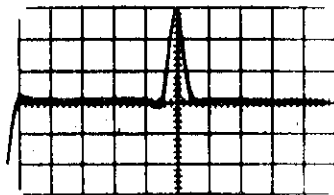
Unshielded Probe Head #57  
150 ma Record Current  
10 microseconds/cm, 5 mv. /cm  
Spread: 0.018" (at 20% level)

Figure 2B



Ferrite Probe Head  
Same test conditions

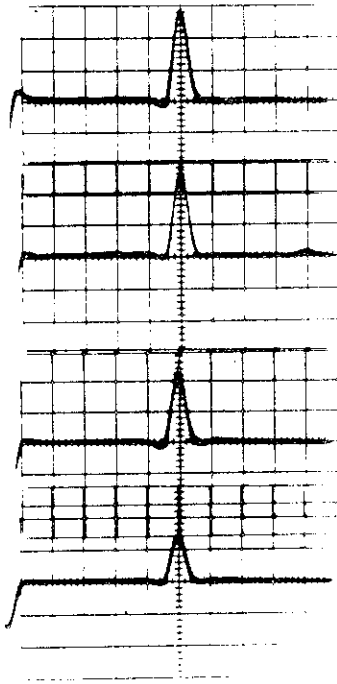
Figure 2C



Shielded Probe Head #62  
Same test conditions  
Spread: 0.007" (at base)

Figure 3A

Shielded Probe Head #62  
10 microseconds/cm; 5 mv/cm.



Record Current: 200 ma.

Record Current: 150 ma.

Record Current: 100 ma.

Record Current: 50 ma.

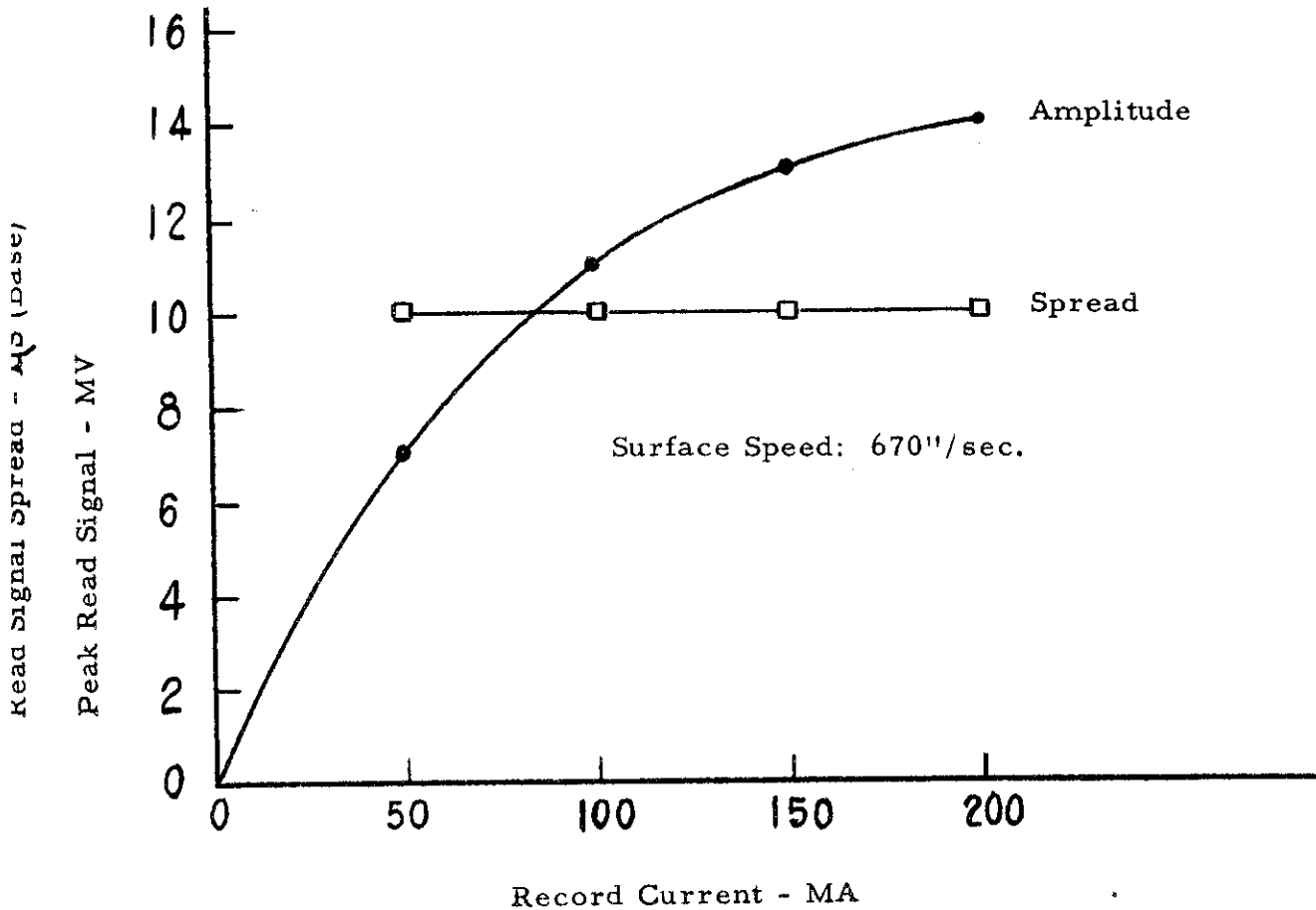


Figure 4

Shielded Probe Head #62

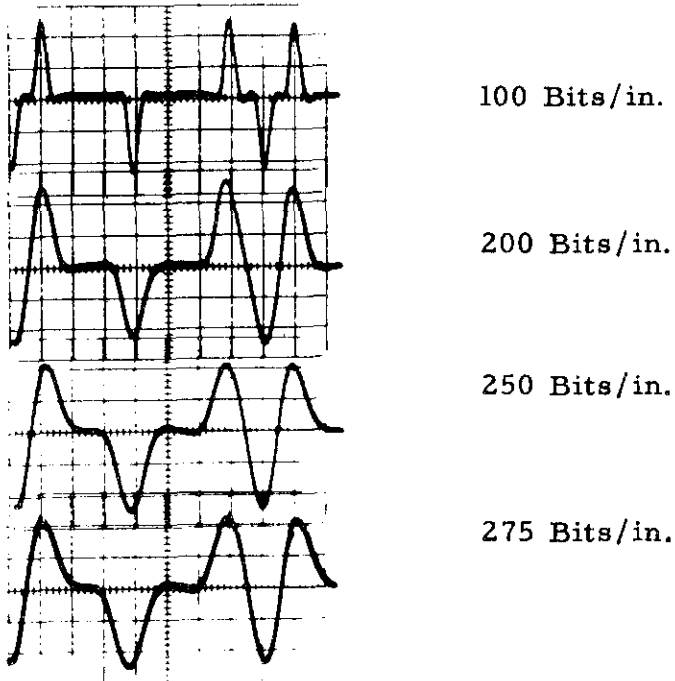




Figure 5A

Read Signals from Tracks .025" Apart

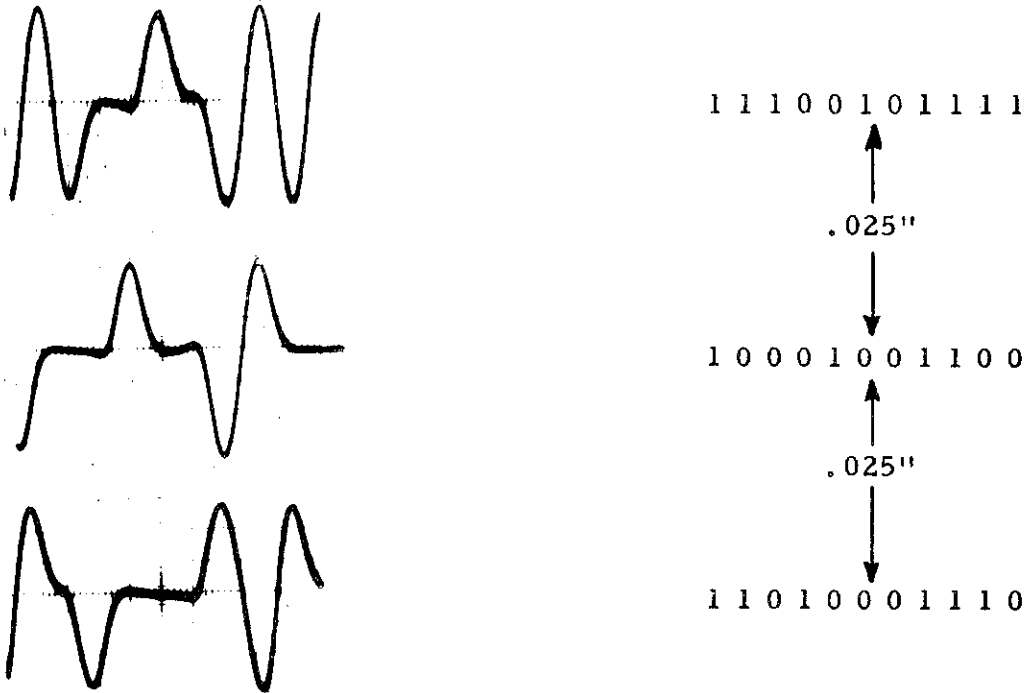


Figure 5B

Read Signals from Tracks .010" Apart

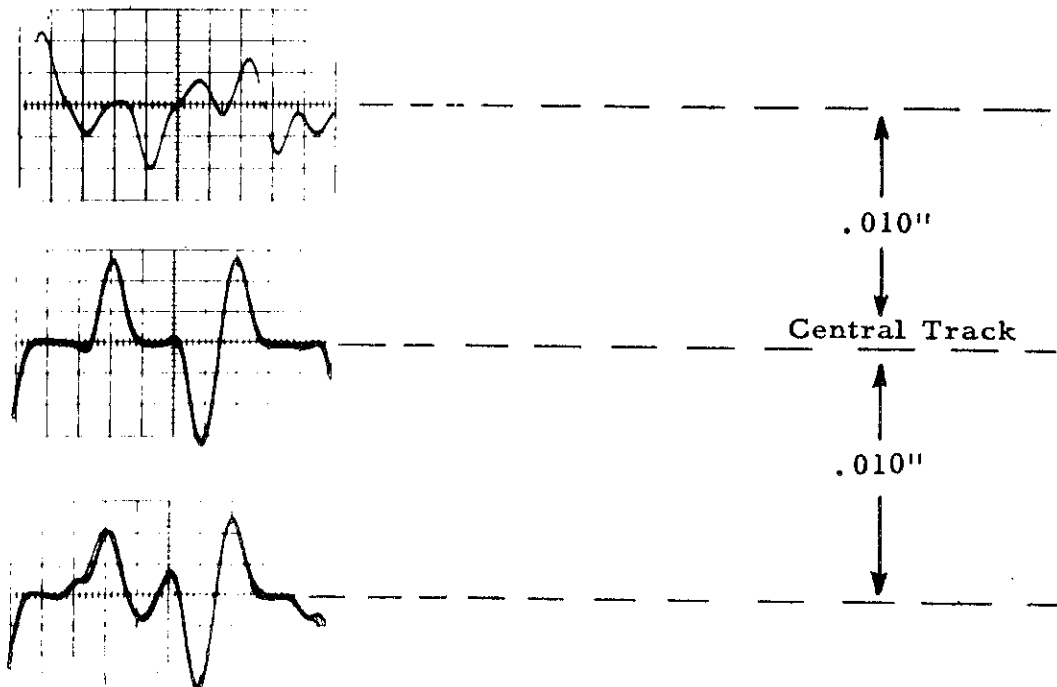
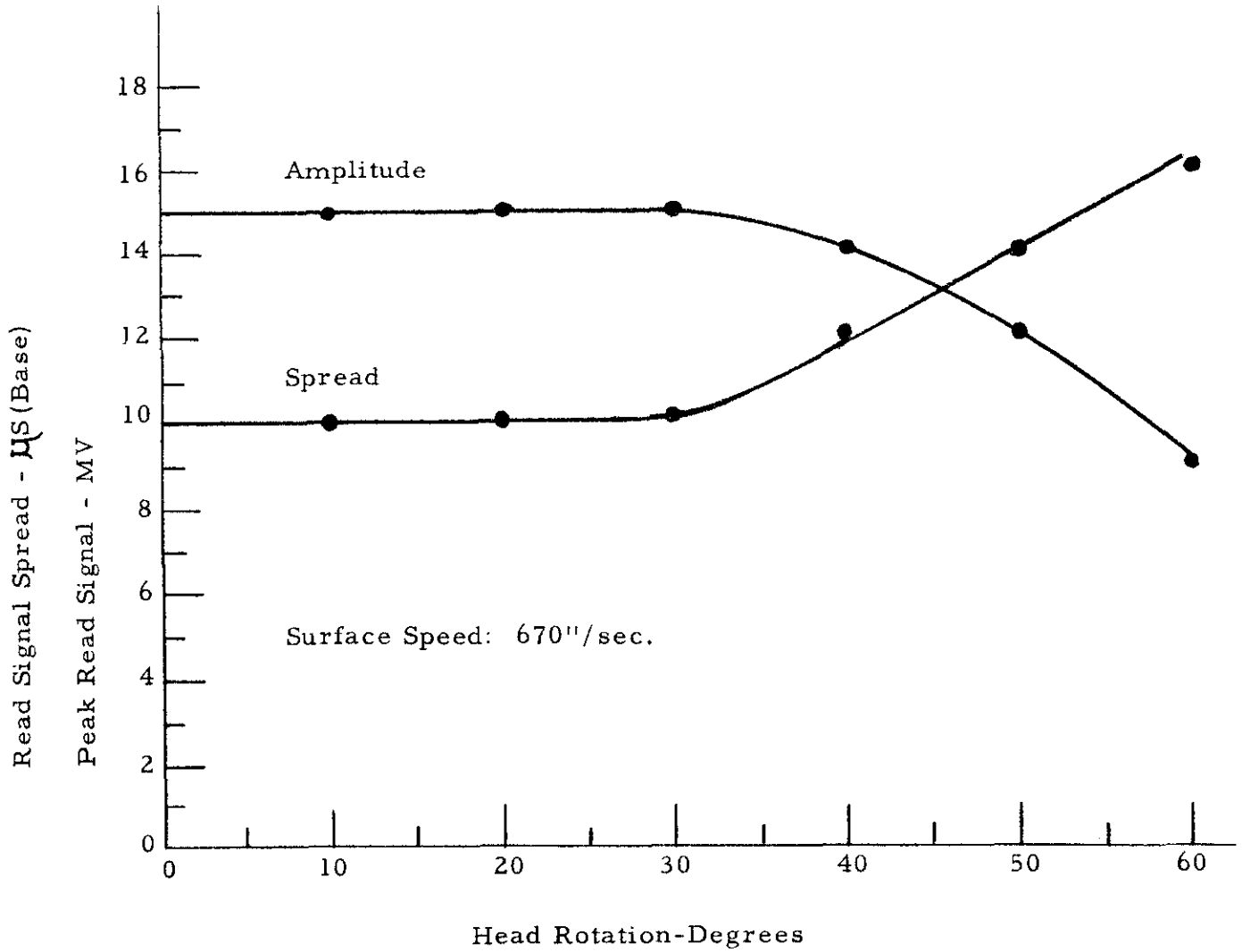


FIGURE 6



APPENDIX A

Field Pattern of Stationary Head

An early model of a perpendicular head having shield faces with closed magnetic paths is shown in figure 7. An approximate flux plot of the magnetic field of this perpendicular is plotted in figure 8. The flux plot was made as follows:

- (1) A first approximation of the reluctance of the head was calculated. Extrapolated values of the permeability for 360 kc/s were used for the magnetic materials.
- (2) This reluctance value was used to establish trial values of magnetic potential along the center line of the core in the gap, across the oxide, and through the return path.
- (3) The magnetic equipotential lines were adjusted by the method of curvilinear squares. <sup>1</sup>

The flux plots were required to satisfy the following boundary conditions:

$$\begin{aligned} \overline{n} \cdot \overline{B}' &= \overline{n} \cdot \overline{B}'' \\ \frac{1}{\mu'} (\overline{n} \times \overline{B}') &= \frac{1}{\mu''} (\overline{n} \times \overline{B}'') \end{aligned} \tag{A. 1}$$

These quantities are defined in Stratton <sup>2</sup> for the transition between two media designated by prime and double prime. For two-dimensional problems, the ratio of the length to width of the curvilinear rectangles is:

$$\frac{\int_{L_j}^L \mu_i}{\int_{L_j}^L \phi_j} = \frac{\int_{L_j}^L \mu_i}{\int_{L_j}^L \phi_j} = k\mu \tag{A. 2}$$

The distance along a flux line  $\phi$  or a magnetic potential line  $U$  are designated by  $\int_{L_j}^L \phi$  and  $\int_{L_j}^L \mu$ . The permeability of the medium divided by the vacuum permeability is defined as  $\mu$ . The constant,  $k = 1$ , in this analysis.

1 E. Weber. Electromagnetic Fields Vol. (1950) pp 201-204

2 J. A. Stratton Electromagnetic Theory (1941), Section 1.13

At saturation, such as in the oxide layer near the center line of figure 8, a value of  $\mu = 2$  is assumed. The relationship between  $\overline{B}$ ,  $\overline{H}$ , and  $\overline{M}$  is given by:  $\left\{ \begin{array}{l} \mu = 1 + (\overline{M}/\overline{H}) \\ \overline{B} = \mu_0 (\overline{H} + \overline{M}) = \mu \mu_0 \overline{H} \end{array} \right.$  (A. 3a)

(A. 3b)

Substitution  $\mu = 2$  in (A. 3a) above gives in the oxide:

$$2 = 1 + (\overline{M}/\overline{H}) \text{ or } \overline{H} = \overline{M}$$

Substitution in (A. 3b) gives  $\overline{B} = 2 \mu_0 \overline{M}$ , (A. 4)

It has been assumed that the magnetizing force  $\overline{H}$ , and the magnetization  $\overline{M}$  are in the same direction. The free space magnetic permeability is  $\mu_0 = 4\pi \times 10^{-7} \frac{\text{henries}}{\text{meter}}$ .

If the static head in figure 8 is removed from the oxide disk, a fraction of the field due to the ampere turns on the head is taken away. In this case where we assumed  $\mu = 2$  in the oxide, half the field is removed, leaving

$$\overline{B}^1 = \mu_0 \overline{M}^1 \text{ in the oxide, and } \quad (A. 5)$$

$$\overline{B}^1 = \mu_0 \overline{H}^1 \text{ in the air above the oxide. } \quad (A. 6)$$

At the surface the normal components of  $\overline{B}$  are equal making  $\overline{M}^1 = \overline{H}^1$  where  $\overline{M}^1 = \overline{H}$ , the magnetizing force in ampere-turns per meter in the oxide from the flux plot of figure 8.

Using equation (A. 4) and (A. 5) and  $\overline{M}^1 = \overline{M}$  since the removal of the head is assumed to be done without changing the magnetization in the oxide, gives:  $\overline{M}^1 = \overline{B} / 2 \mu_0$ . (A. 7)

This reduction of  $\overline{B}$  by a factor of two from figure 8 to figure 9 is accomplished by increasing the thickness of the slice which the flux plot represents by a factor of  $\sqrt{2}$  and by increasing the separation of the flux lines by a factor of  $\sqrt{2}$ . Each tube of flux is still  $3.8 \times 10^{-4}$  Maxwells.

Recorded information is read from the voltage induced in the head by cutting the flux of this field. The value of this flux is taken graphically

from figure 8 and is plotted in figure 9. For the plane .0005" above the surface; the sensitivity curve is replotted in figure 10 for several values of magnetizing current on writing. The curves of figure 10 are interpolated linearly on the assumption that the magnetic field intensity does not reach saturation in the oxide layer, which is not strictly correct. The accuracy of the flux plot depends upon:

1. The degree of correctness of the boundary conditions. In this case the terminating boundary values of magnetic potential were based on trial calculations of reluctance.

2. The accuracy of the assumed values of magnetic permeability in the core, oxide, shield, and iron disk.

3. The degree to which the flux plot satisfies.

Laplace's equation:

$$\nabla^2 U = 0, \quad (A.8)$$

where U is the magnetic potential or m.m.f. in ampere-turns.

4. The extent to which the relative permeability,  $\mu$  calculated from equation (A.2) for a region of the flux plot agrees with the assumed values of  $\mu$ .

The flux plot made by a freehand drawing in of curvilinear rectangles, can be checked for condition (3) by use of the basic formula from the relaxation method.\* Two points in the flux plot of figure 8 are checked by the formula:

$$\% \text{ Error} = \frac{U_1 + U_2 + U_3 + U_4 - U_0}{4U_0} \times 100 \quad (A.9)$$

\* E. Weber. Electromagnetic Fields Vol. I (1950) pp.259-270

Parts A and B in the flux plot of figure 8 are checked by use of equation (A. 9) and are found to have errors of 0.07% and 2.3% respectively.

Points C, D, E, and F in the flux plot are checked by condition 4, i. e., the relative permeability is checked from the flux plot by use of equation (A.2) with  $k = 1$ . The results are tabulated below:

<u>Point</u>	<u>Calculated <math>\mu</math></u>	<u>Assumed <math>\mu</math></u>
C	164	200
D	18.4	6
E	5.1	6
F	1	1

Examination of the above table shows that the plot is reasonably consistent except in the region around D, where further adjustments should be made.

In Figure 11, a longitudinal magnetic recording head is compared with a perpendicular head by use of the flux plot of figure 8 and a flux plot made by L. H. Bixby.\*\* This comparison is made for a writing density of 120 bits per inch. In this range of bit density the perpendicular head has thirty per cent of the flux in the oxide compared to three per cent for the longitudinal head. The perpendicular head also has the advantage of lower inductance. When higher bit densities are required, the perpendicular head eventually reaches a limiting density above which longitudinal heads would be required. This change-over point would be at the limit on the minimum thickness of the core of the perpendicular head, because it is possible to make smaller gaps than cores, and the saturation density of the core material reduces the total flux as the core thickness is decreased.

\* E. Weber. Electromagnetic Fields Vol. I (1950) pp.259-270

\*\* L. H. Bixby "Investigations of Magnetic Recording" 6-30-54 page 9

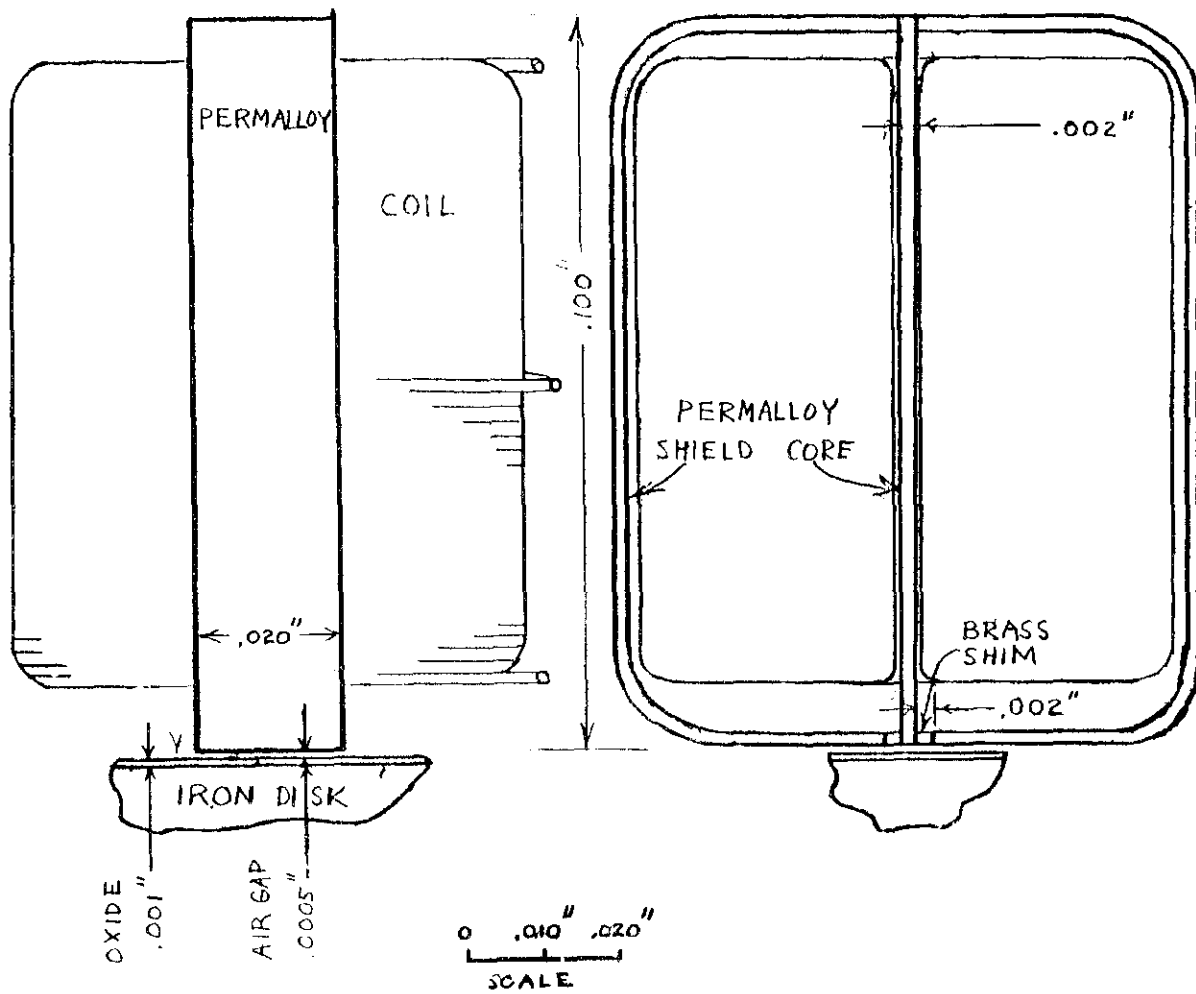
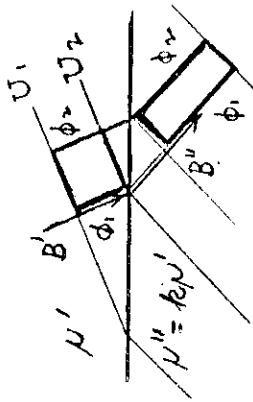
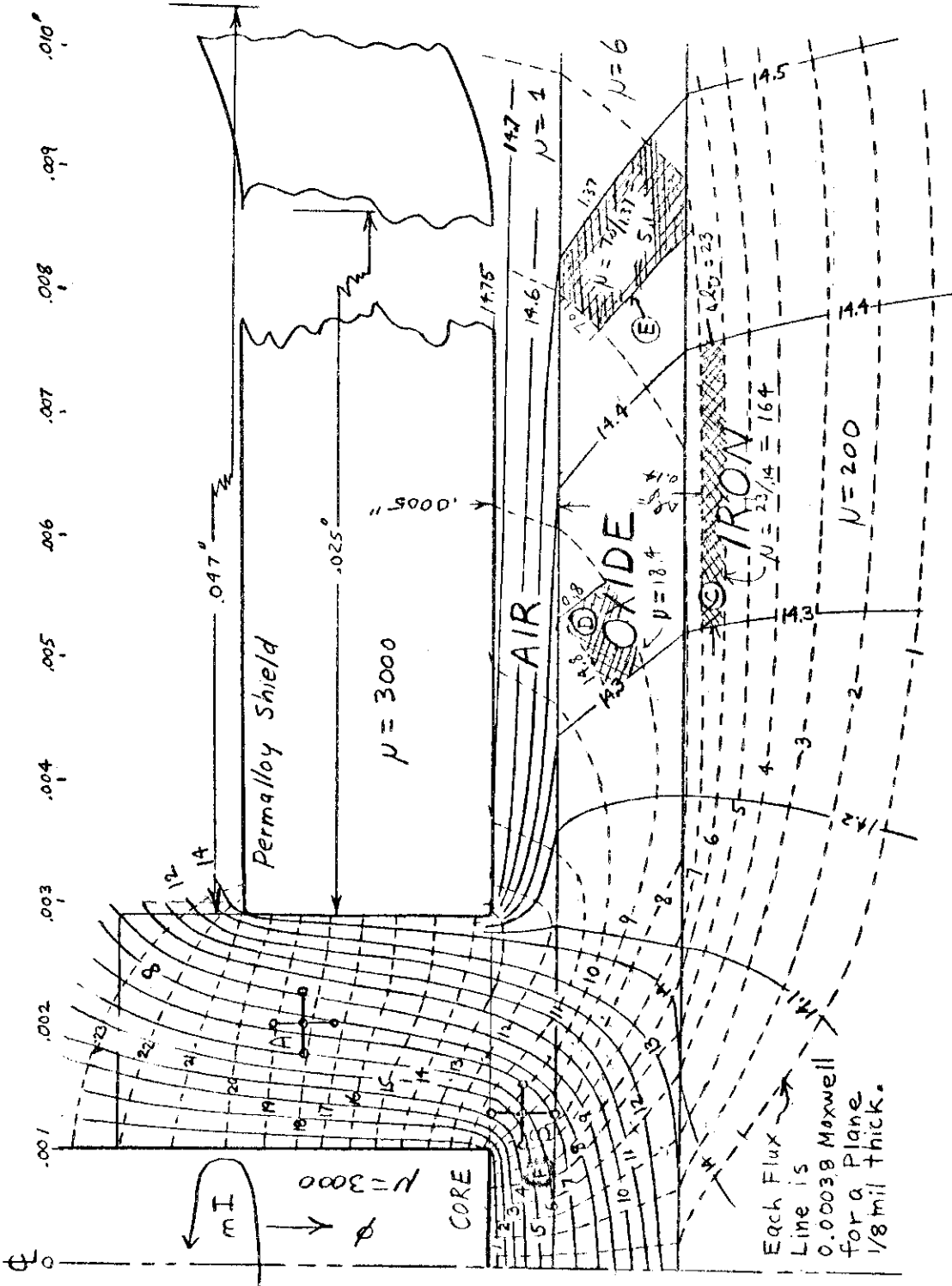


FIGURE 7 - PERPENDICULAR HEAD WITH CLOSED RETURN SHIELD



CURVILINEAR RECTANGLES

Point A: +0.07%  
 $U_4 = 7.5$  error  
 $V_0 = 7.6$   
 $U_3 = 6.0$   $U_1 = 9.1$   
 $U_2 = 8.0$

Point B: +2.3% error  
 $U = 4.5$   $5.5$   $7.0$   
 $7.0$

NET POINT  
 (RELAXATION)  
 METHOD

FIGURE 8 - FLUX PLOT

Each Flux Line is 0.00038 Maxwell for a Plane 1/8 mil thick.



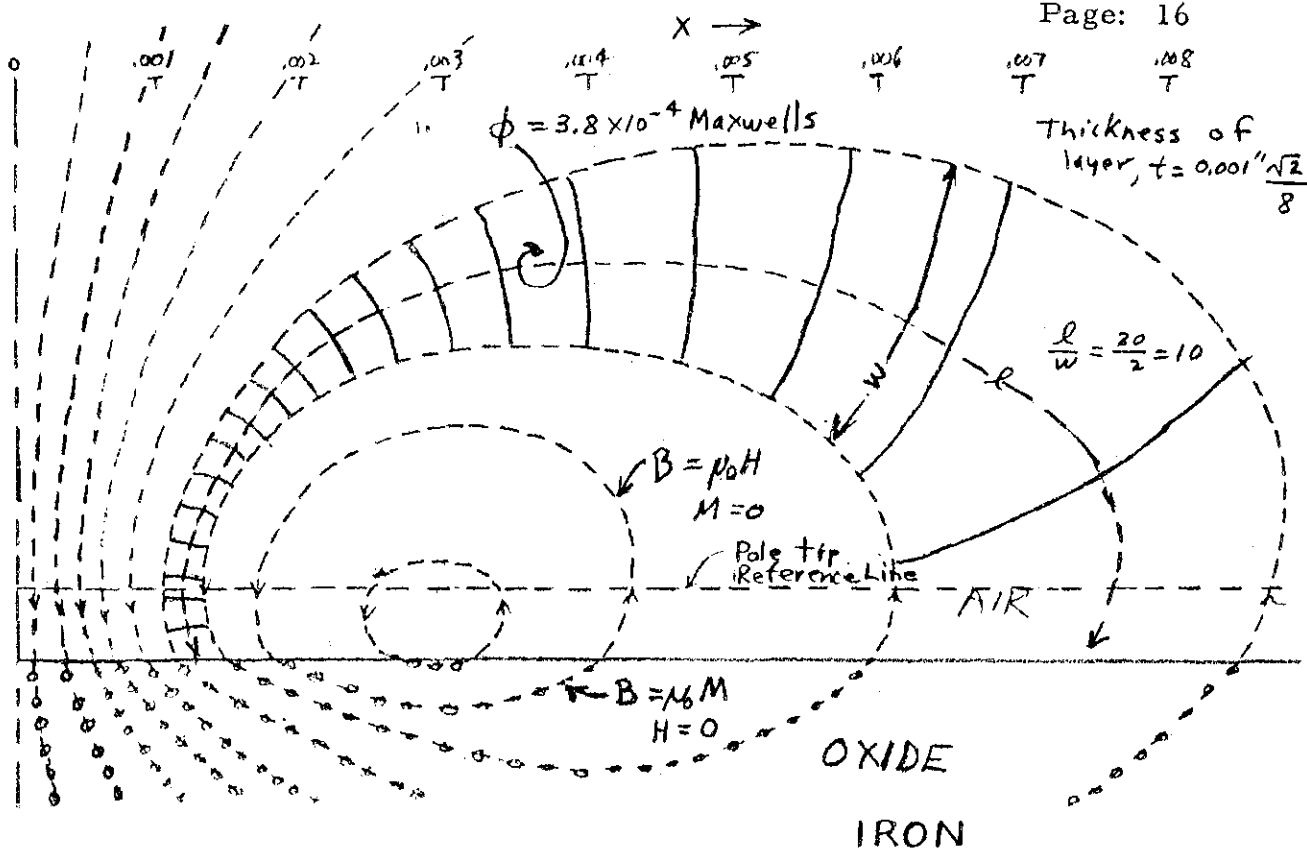


FIGURE 9 - RESIDUAL MAGNETIC FIELD AFTER STATIC WRITING

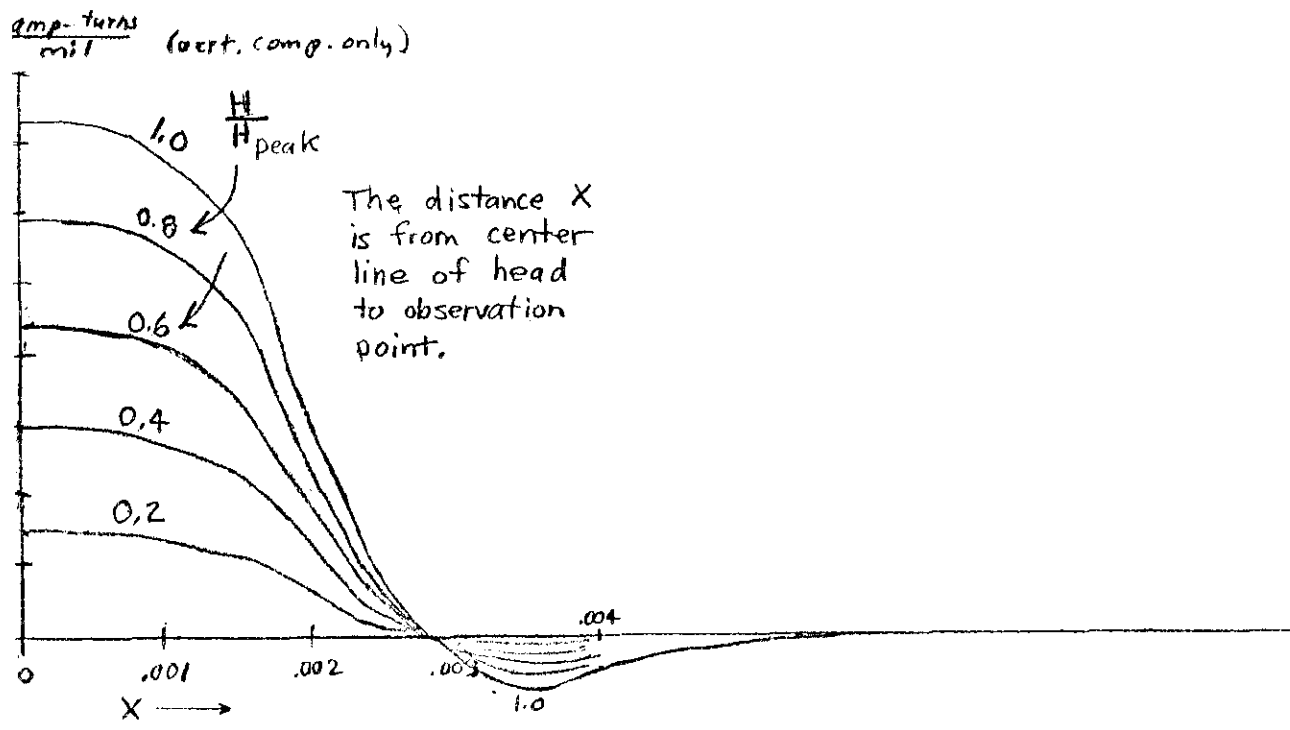


FIGURE 10 -  $H$  vs.  $X$  for SHIELDED RETURN PATH


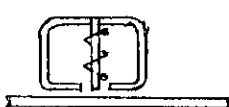
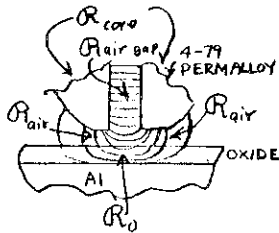
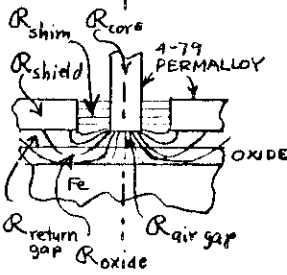
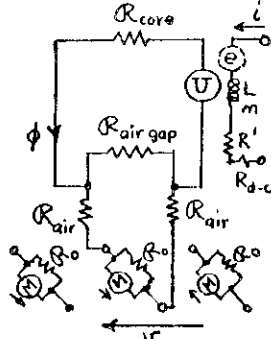
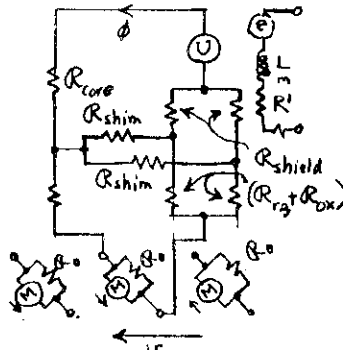
	LONGITUDINAL	PERPENDICULAR
Recording Head:	Delta Type 	#18 
Reference Flux Plot:	L. H. Bixby, Jr. "Investigation of Magnetic Recording 6/30/54 (unpublished notes) page 9, figure 7.	Appendix A of this report Figure 8
Number of lines through oxide layer:	7	7
Number of lines through air gap and returnpath:	202	16
Percentage of lines through useful region of oxide storage layer:	3.3%	30%
Detail of structure at recording gap:		
Approximate equivalent circuit:		
Principal Oxide Layer:		
$R = \sum \frac{l}{\mu A}$ (henry <sup>-1</sup> )		
Approximate reluctance values:		
Core area:	$24 \times 10^{-8} \text{ m}^2$ (.020" x .020")	$2.4 \times 10^{-8} \text{ m}^2$ (.002" x .020")
$R_{\text{Core}}$	$19.5 \times 10^6$	$27 \times 10^6$
$R_{\text{Series air gap}}$		$520 \times 10^6$
$R_{\text{Shunt air gap}}$	$156 \times 10^6$	$841 \times 10^6$
$R_{\text{Oxide}}$		$450 \times 10^6$
$R_{\text{Total}}$	$180 \times 10^6$	$1190 \times 10^6$
Saturation flux: $\Phi = BA$	$0.6 \times 24 \times 10^{-8} = 14.4 \times 10^{-8}$ webers	$1.44 \times 10^{-8}$ webers
$U = nI = \Phi R$ for saturation of core (oxide already saturated)	$14.4 \times 10^{-8} \times 180 \times 10^6 = 26$ amp-turns	$1.44 \times 10^{-8} \times 1190 \times 10^6 = 17$ amp-turns
turns, n	250	175
current, I	0.100 amp	0.100 amp
reference density (bits per inch)	120 NRZI	120 NRZI
frequency	180 kc (1, 1, 1, 1, 1)	180 kc (1, 1, 1, 1, 1)
surface velocity	1.5 mil / $\mu$ sec	1.5 mil / $\mu$ sec
Inductance, $L = \frac{n^2}{R}$	$\frac{250^2}{180 \times 10^6} = 350 \times 10^{-6}$ henries	$\frac{175^2}{1190 \times 10^6} = 26 \times 10^{-6}$ henries
Reactance $X = \omega L$		
$\omega = 2\pi f = 2.26 \times 10^6$	$2.26 \times 350 = 790$ ohms	$2.26 \times 26 = 59$ ohms

FIGURE 11 - COMPARISON OF LONGITUDINAL AND PERPENDICULAR HEADS

## APPENDIX B

### Estimate of Magnetization levels and reading Voltage

#### Permeability of Materials

The permeability of the 4-79 Mo-permalloy used in the core and shields has been estimated as 3000 by extrapolating from the manufacturers' curves\* for initial permeability for a frequency of 360 kc/s.

Two hysteresis curves are plotted in figure 12 for the oxide. The solid curve is for Minnesota Mining & Manufacturing Co. oxide tape type BQ. The dashed curve is for red  $\text{Fe}_2\text{O}_3$  powder supplies by C. K. Williams Co. and has been estimated from the values of  $B_r$  and  $H_c$ .

A straight line approximation to the hysteresis curve for red  $\text{Fe}_2\text{O}_3$  is given in figure 13. This straight line approximation to the hysteresis curve causes a serious distortion of the calculated magnetization levels due to the inaccurate slope at  $H = 0$ . However, the inaccurate hysteresis curve was used to simplify the approximate calculation of the magnetization levels.

#### Writing Magnetization Pattern

The results of a sample calculation of the reluctance of the perpendicular head of figure 7, using the permeabilities indicated in figure 8, are tabulated in figure 11. A trial calculation of the reluctance was made first, followed by

---

\* Arnold Engineering Company Bulletin TC-101A, March 1953, Figure 8 and 11.

a trial flux plot based on it. Then a second reluctance calculation was made which was then followed by an adjustment of the flux plot by the method of curvilinear rectangles illustrated in figure 8. The resultant magnetization pattern in the oxide at a reversal of current in the writing coil is developed graphically point by point in figure 13 as illustrated in figure 14. The mmf distribution through the oxide near the head was taken from figure 10, except that the return flux for  $X < .003''$  as neglected. The time is shown on the accompanying hysteresis curve. A surface velocity of 1.5 mils per microsecond was assumed. The process of magnetization of a particular point in the track is illustrated in figure 14 for the point  $\ell = -0.00075''$  of figure 13. This is the point  $.00075''$  behind the centerline of the recording head at the time the current starts to change. The curve A and B of figure 13 are for the straight line approximation to the oxide hysteresis curve and for the rounded curves respectively. Each point of these curves was traced out graphically from the  $\overline{H}(\ell)$  curves on the right portion of figure 13 as projected on the hysteresis curves on the left side. Resultant values of  $\overline{B} = \mu_0 \overline{M}$  are read off of the hysteresis curve and are replotted on the right side of figure 13. The circled numbers on the hysteresis curve in figure 13 correspond to the time scale of figure 14. Current reversal time of one microsecond was used. The magnetization versus position along the track is compared for two cases in figure 15.

The curve "neglecting return flux" is copied from figure 13 case A. The curve "with residual flux" was constructed in a similar manner, but with the complete return flux pattern of figure 10 utilized. For case A the length of one magnetization reversal is:  $\Delta \ell_A = .0014''$ . The undistorted potential writing bit density is:  $D = 1/\Delta \ell_A = 1/.0014'' = 700 \text{ bits/inch}$ . Curve C yields a potential writing density of:  $D = 1/.0075'' = 400 \text{ bits/inch}$ .

Since the approximate hysteresis curve of figure 13 has too high a slope at  $H=0$ , the potential writing density should be higher than 400 bpi, even with a concentrated return flux.

### Reading Waveform

The real significance of the writing density will not be apparent until the effect upon reading waveforms is estimated. To calculate the reading voltage at the head from:

$$V = \frac{d\phi}{dt}, \quad (B.1)$$

it is necessary to calculate the effective mmf as a function of time by use of the  $M(x)$  curve of figure 15, the reciprocity theorem\*, the  $H(L)$  curve of the head of figure 10, the hysteresis curve of the core, and the reluctance of the rest of the magnetic circuit. If the above information is available giving a  $\phi(t)$  in the head core, then the reading voltage can be obtained by differentiating  $\phi(t)$ .

### Reciprocity Relation

Using the reciprocity relation in the form used by Hoagland,\* and defining a sensitivity function:

$$h_y(x) = \frac{H}{H_p} \quad (B.2)$$

from figure 10, the flux in the core of the head is approximately:

$$\phi_{xy}(\bar{x}) = K \int_{-\infty}^{+\infty} M_y(x-\bar{x}) h_y(x) dx \quad (B.3)$$

The coordinates are defined in figure 16.

Here the horizontal components of the magnetization  $M$  are neglected:

$$d\phi(x) \text{ (amp-t)} = \frac{\ell M}{R(x)} \frac{(x-\bar{x})}{w} \frac{\text{(amp-t)} h(x) dx \text{ (in)}}{\text{(in)}}$$

The mmf in the head disk magnetic circuit is obtained by integrating:

$$\phi(x) = \int_{-\infty}^{+\infty} \frac{M(x-x)}{R(x) w} h(x) dx \quad (B.4)$$

\* L. Brillouin "Magnetic Recording Theory of the Recording Head" 11/22/49, pp. 1-48.  
 A. L. Hoagland "Magnetic Recording-Head Design for Disk Storage 9/24/54, pp. 3-5.  
 202.111.066.

$$\tilde{M}(x-\bar{x}) = M(x-\bar{x}) \ell \quad (\text{amp-t}) \quad (\text{B.5})$$

$\ell$  = thickness of oxide layer (in)

$w$  = unit width (in)

$$K = 1/R w$$

For reading, assume  $R(\bar{x})$  is a constant to get a first approximation. This is reasonable for the core of this head because the flux is below saturation on reading. However, this neglects the variation of  $\mu(\xi)$  in the oxide coating, which may have to be considered in better approximations. Noting that the  $K$  in equation (3) is reciprocal reluctance per unit width:

$$\phi_2(\bar{x}) = \frac{1}{Rw} \int_{-\infty}^{+\infty} M_y(x-\bar{x}) h_y(x) dx, \quad (\text{B.6})$$

$h_y(x)$  from figure 10.  $M_y = B_r/\mu_0$  from figure 13.

$$\phi_2(\bar{x}) = \frac{1}{R} (\text{henry}^{-1}) \int_{-\infty}^{+\infty} M_y(x-\bar{x}) \left[ \frac{\text{amp-t}}{\text{mil}} \right] h_y(x) dx (\text{mil})$$

webers  
for  $x, \bar{x}$ , in mils where  $w = 1$  (mil)

$$M = \frac{B_r}{\mu_0} = \frac{.155 (\text{weber/meter}^2) \cdot 2.54 (\text{cm/in})}{4 \times 10^{-7} (\text{henries/meter}) \cdot 10^2 (\text{cm/meter}) (\text{amp-t/in})} = 3130$$

The maximum  $M$  in figures 13 and 14 is 3.13 (amp-t/mil.)

This is 2.02 (amp-turn/mil) of  $M$  per 1 (kilogauss of)  $B_r$ .

Referring to figure 11 for the total reluctance  $R = 1190 \times 10^6$  (henry<sup>-1</sup>) and  $R' = 2R = 2.37 \times 10^9$  (henry<sup>-1</sup>).

Noting that  $h_y(x) = 0$  for  $(x) \geq .003''$  permits cutting off the limits of integration where  $w = 2a$  (mils)

$$\phi(x) (\text{webers}) = \int_{-a}^{+a} \frac{\ell (\text{mils}) M_y(x-\bar{x}) \left[ \frac{\text{amp-t}}{\text{mil}} \right] h_y(x) dx (\text{mil})}{R' (\text{henry}^{-1}) \cdot 2a (\text{mil})} \quad (\text{B.7})$$

The induced voltage is: 
$$e_i = n \frac{d\phi}{dt} = n v \frac{d\phi}{dx} \quad (\text{B.8})$$

This requires integration with respect to  $x$  and differentiation with respect to  $\bar{x}$ .

### Numerical Integration

Changing equation (7) from an integral to a sum gives:

$$\phi(\bar{x}) = \sum_{i=-n}^{i=+n} \frac{\ell M_y(x_i; \bar{x}) h_y(x_i) \Delta X}{R'' (2n+1) \Delta X} \quad (\text{B.9})$$

$x_i = x$  in center of interval  $\Delta X_i$

For computation, terms can be rearranged:

$$\phi(\bar{x}) = \frac{l}{(2n+1)R} \sum_{i=-n}^{i=n} M_y(x_i - \bar{x}) h_y(x_i)$$

- $l$  = thickness of oxide layer (mils)
- $R^1$  = reluctance of complete path (henry<sup>-1</sup>)
- $M_y$  = magnetization (amp-t/mil)
- $h(x)$  = gain function (dimensionless)
- $\phi(\bar{x})$  = magnetic flux (webers)

A sample calculation is shown in figure 17.

In figure 18,  $\phi R$  is plotted against  $\bar{x}$  (mils) and  $t$  ( $\mu$  sec). A velocity of 1.5 (mil/ $\mu$  sec) is assumed, which corresponds to an outer track of a RAM disk. For an inner track  $v = 0.75$  (mils/ $\mu$  sec).

Taking the derivative of  $\phi R$  gives the theoretical reading voltage curve. This gives a peak voltage of 0.192 volts at the outer track or 0.096 volts at the inner track. This procedure of calculating the reading voltage sets up a system for calculating the effect of charging parameters in magnetic head design.

The demagnetization effect described by Westmizje \* has not been calculated in this example. For more accurate analysis the demagnetization effect should be investigated.

---

\* W. K. Westmizje "Studies on Magnetic Recording" (1953).

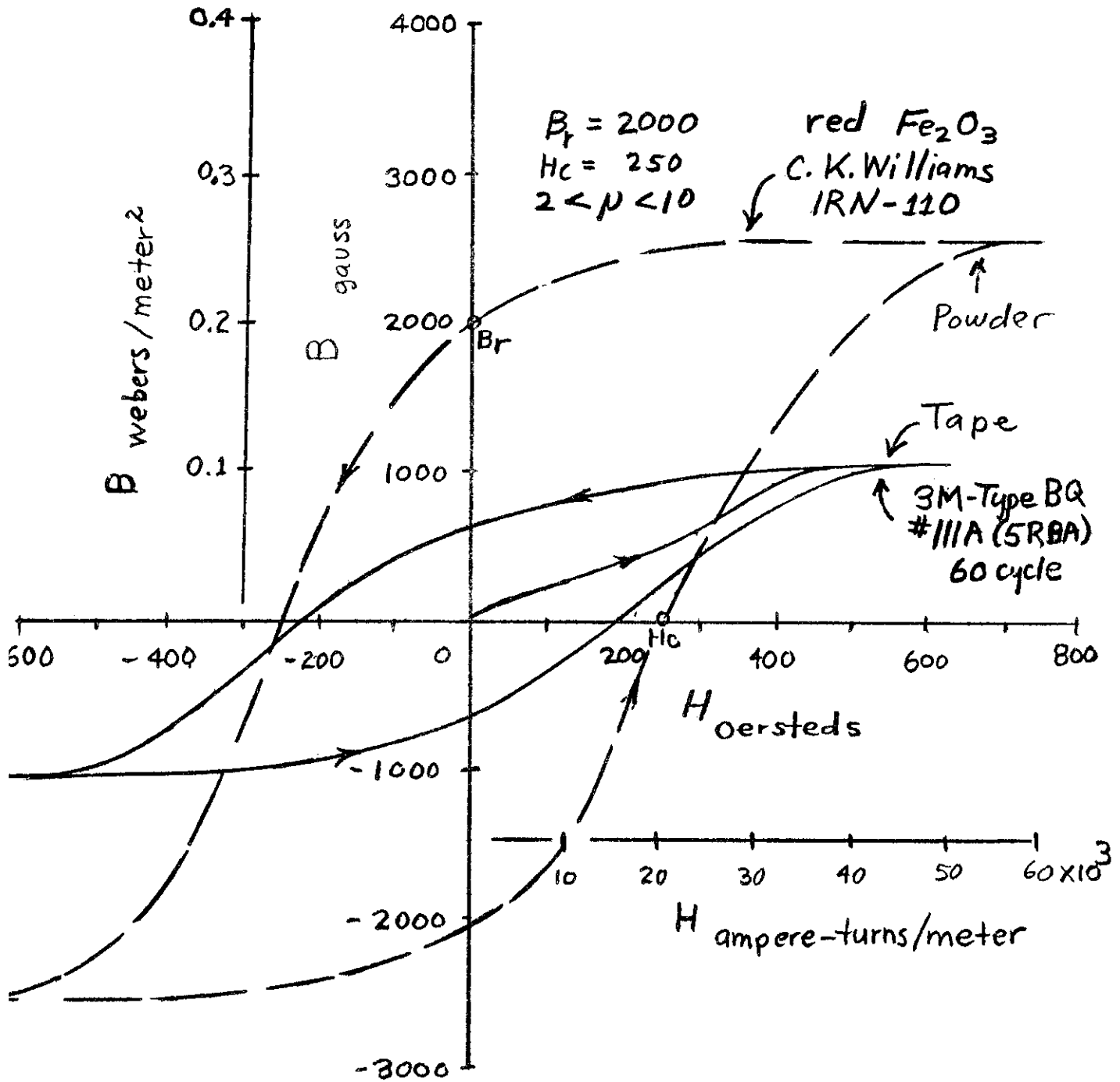


FIGURE 12 - APROXIMATE HYSTERESIS CURVES FOR OXIDE



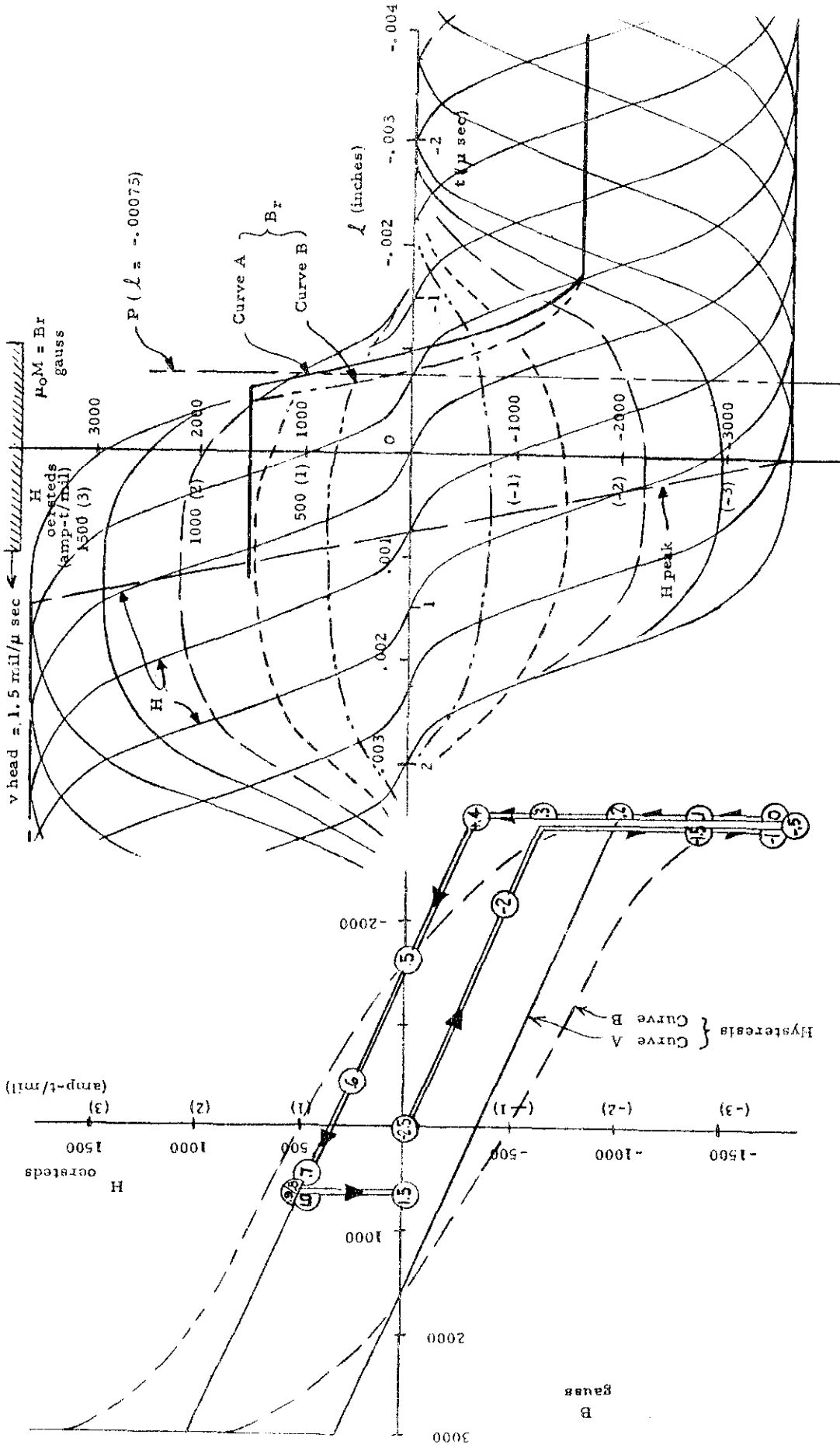


FIGURE 13 - WRITING MAGNETIZATION CURVES

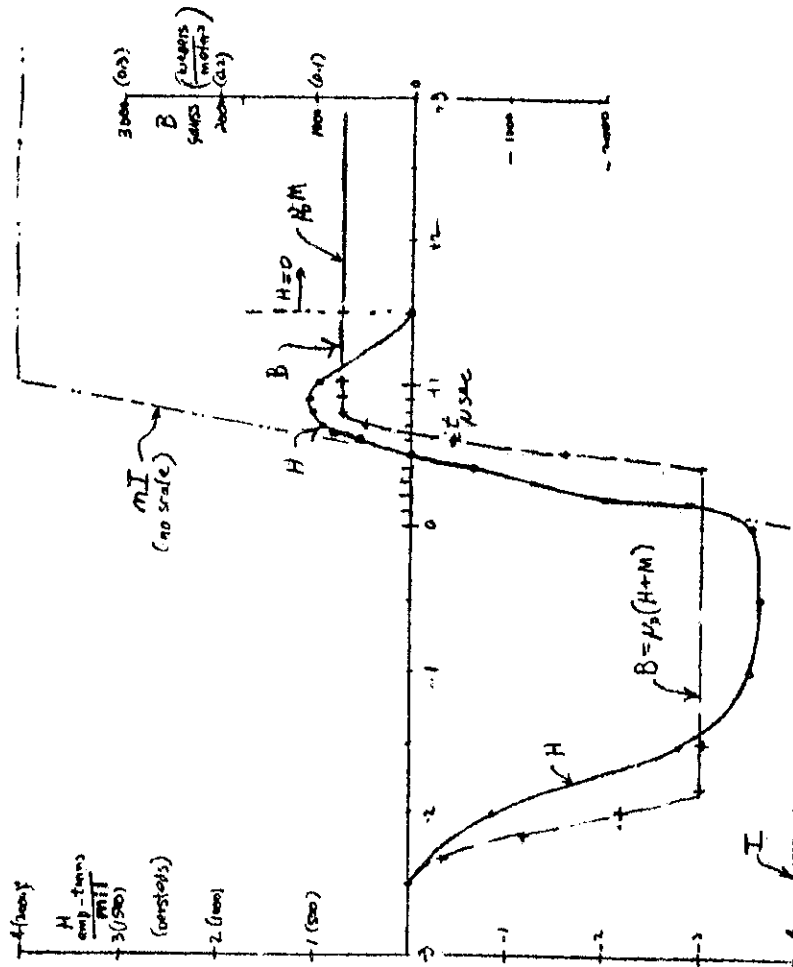


FIGURE 14- B, H, and M as a FUNCTION of TIME for the POINT P ( $\ell = -0.00075''$ ).

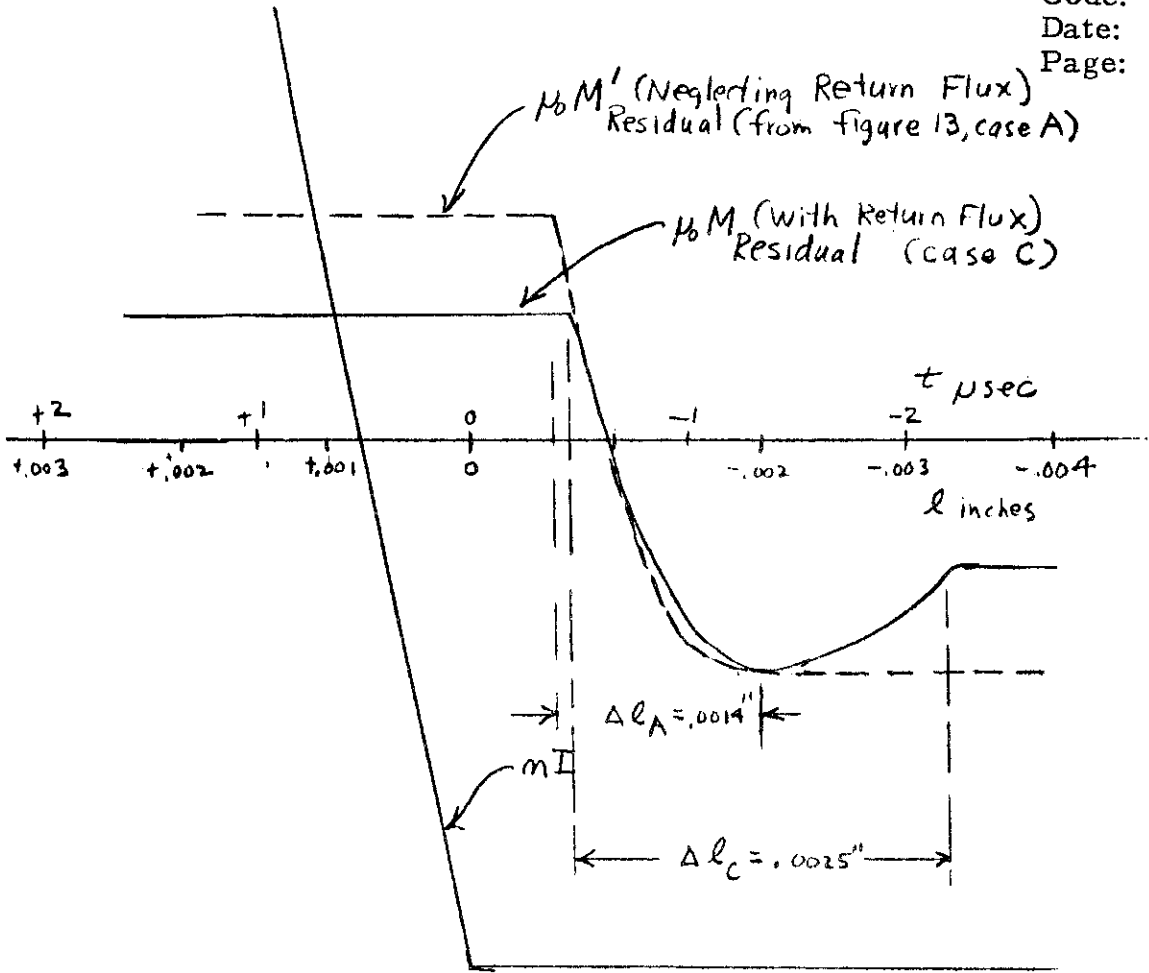


FIGURE 15 COMPARISON OF RESIDUAL MAGNETIZATION CURVES WITH AND WITHOUT RETURN FLUX.

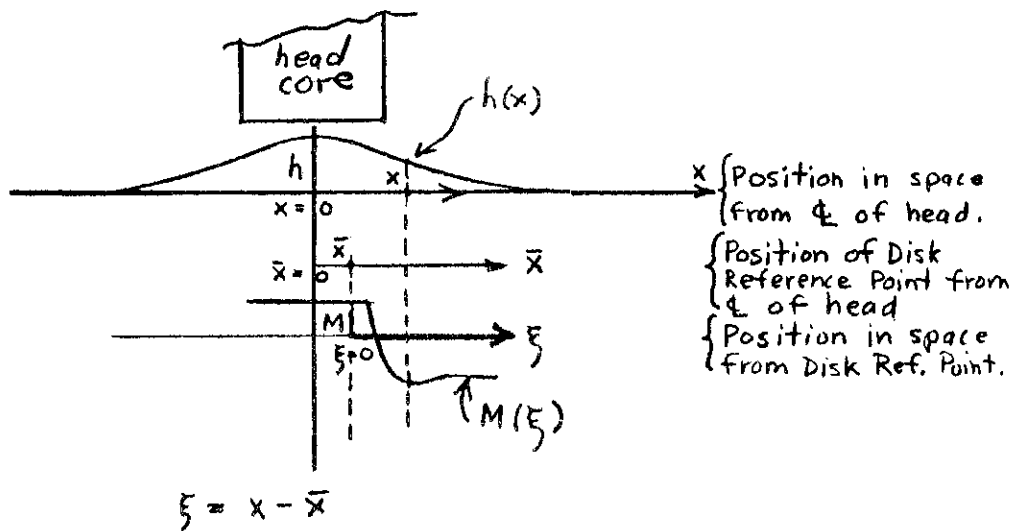


FIGURE 16 - COORDINATE SYSTEM

$\xi = x - \bar{x}$	$My(\xi)$	X	hy(x)	$M_{max} h_y$	$\bar{x} = -2.000$	X	( $\xi$ )	$Myhy$	5 term sum sum $Myhy$
-3.0	+3.10	0	1.00	3.100	-3.0				0.372
to		$\pm .1$ to 5	1.00	15.500	-2.6				
0		$\pm .6$	.99		-2.5				3.626
to		.7	.98		-2.1				
+0.6	+3.10	.8	.97	14.931	-2.0				8.926
		.9	.95		-1.6				
0.7	2.40	1.0	.93		-1.5	+0.5	2.480		
0.8	1.40	1.1	.91		1.4	0.6	3.070		
0.9	0.60	1.2	.89					9.434	
1.0	-0.20	1.3	.87	13,292	1.3	0.7	2.090		
1.1	-0.80	1.4	.82		1.2	0.8	1.248		
1.2	-1.40	1.5	.80		-1.1	0.9	0.546		
1.3	-1.90	1.6	.75		-1.0	1.0	-.186		
1.4	-2.40	1.7	.68		-0.9	1.1	-.760		
1.5	-2.70	1.8	.59	8.926	-0.8	1.2	-1.359		-6.545
1.6	-2.90	1.9	.45		-0.7	1.3	-1.862		
		2.0	.41		-0.6	1.4	-2.378		
1.7	-3.10	2.1	.38		-0.5	1.5	-2.700		
on		2.2	.30		0.4	1.6	-2.900		
		2.3	.25	3.626					
		2.4	.14		0.3		-3.100		-14.900
		2.5	.10		0.2		-3.100		
		2.6	.06		0.1		-3.100		
		2.7	.03		0				-3.100
		2.8	.02	.372	+0.1				-15.500
		2.9	.01		+0.5				
		3.0	0		+0.6				
					+1.0				-14.921
					+1.0				
					+1.5				-13.292
					+1.6				
					+2.0				-8.926
					+2.1				
					+2.5				-3.626
					+2.6				
					+3.0				-0.372
									-58.834

Total less zero 56.647

$(2n+1) = 61$

$$\left[ \frac{\text{henry}}{\text{sec}} \right] = \frac{n[\text{turns}] v[\text{mils}/\mu\text{sec}]}{10^{-6}[\text{sec}/\mu\text{sec}] R[\text{henry}^{-1}]} \frac{\partial U[\text{amp-t}/t]}{\partial \bar{x}[\text{mil}]}$$

$$= \frac{150 \times 1.50}{10^{-6} \times 2.37 \times 10^9} \times 2 = .190 \text{ volts}$$

Point "T" of Figure 18.

$$\Phi(-2)R = -0.964 \text{ for}$$

Point "S" on figure 18.

Figure 17 Tables for Numerical Integration and Sample Calculation.

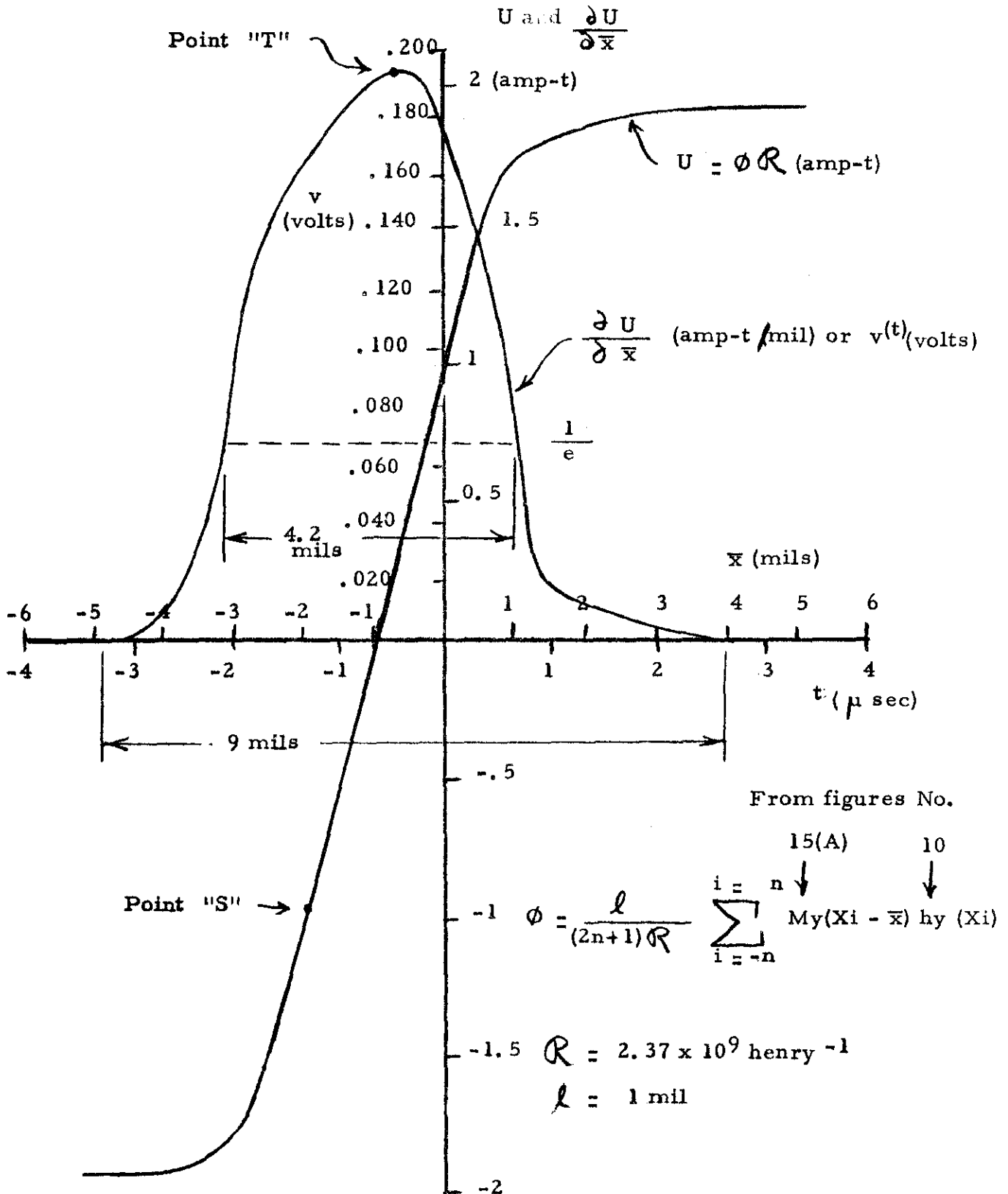


FIGURE 18 MMF and Derivative Obtained by Numerical Integration.

APPENDIX C

A comparison of Magnetic Path Reluctance for Shield Strips  
 and Shield Faces.

The flux plot of Appendix A was started while the experimental work was being conducted with the metallic return path of permalloy strip as shown in figure 7. As the experimental work proceeded, the permalloy shield faces with an air return path as shown in figure 1 were used. The flux plot was not recalculated for the new shields, because the following analysis showed that the reluctance of the return path of the new style shields did not seriously change the total reluctance.

For the return path shield of figure 7, a trial calculation of the total reluctance on writing is as follows:

$$\mathcal{R} = .833 \times 10^6 \text{ henry}^{-1} \left\{ \begin{array}{l} \text{Core Air Oxide Oxide Shield} \\ 33 + 500 + 167 + 1/2 [60+17+50+58] \end{array} \right\}$$

MKS ↑ iron air  
parallel shields ( C.1 )

$$\mathcal{R} = .833 \times 10^6 \left\{ 700 + \frac{175}{2} \right\} = .833 \times 10^6 \times 788 = 655 \times 10^6 \text{ henry}^{-1}$$

The contribution of the return shield on one side is  $58 \times 10^6$  (henry<sup>-1</sup>). Since the two sides are in parallel, the total contribution is one half or  $29 \times 10^6$  (henry<sup>-1</sup>).

Considering the air return path between the two round plate shield faces of figure 19, the flux lines are drawn in approximately. The reluctance is:

$$R = \sum \frac{l}{\mu A} = \frac{\text{mmf}}{\phi} \quad (C.2)$$

Setting a unit cube of length x, and area x<sup>2</sup>, with x approaching 0.020" near the center, and counting the lengths and areas gives approximately:

$$l = 5x \quad (C.3)$$

$$A = 4 \times 34 x^2 = 136 x^2 \quad (C.4)$$

then:

$$\mathcal{R} = \frac{5x}{\mu 130 x^2} = \frac{5}{\mu 136 x} =$$

$$\frac{5}{1.257 \times 10^{-8} \text{ h/m } 136 x (.020'') \times 2.54 \times 10^{-2} \text{ m/in}} =$$

$$R = 57.5 \times 10^6 \text{ henry}^{-1} \quad (C.5)$$

Comparing half of (1) and the complete (5), the additional reluctance of the air return path is approximately:

$$\Delta \mathcal{R} = (57.5 - 29) \times 10^6 = 28.5 \times 10^6 \text{ henry}^{-1}$$

The percentage change is then:

$$\% \Delta \mathcal{R} = 100 \times \frac{\Delta \mathcal{R}}{\mathcal{R}_1} = 100 \times \frac{28.5}{655} = 4.3 \%$$

Since this approximate calculation shows that the large hat-type shields with an air path make less than a 5% change in reluctance, the same flux plot and approximate reluctance calculations can be used with both cases.

SCALE 10:1  
(1" = 0.100)

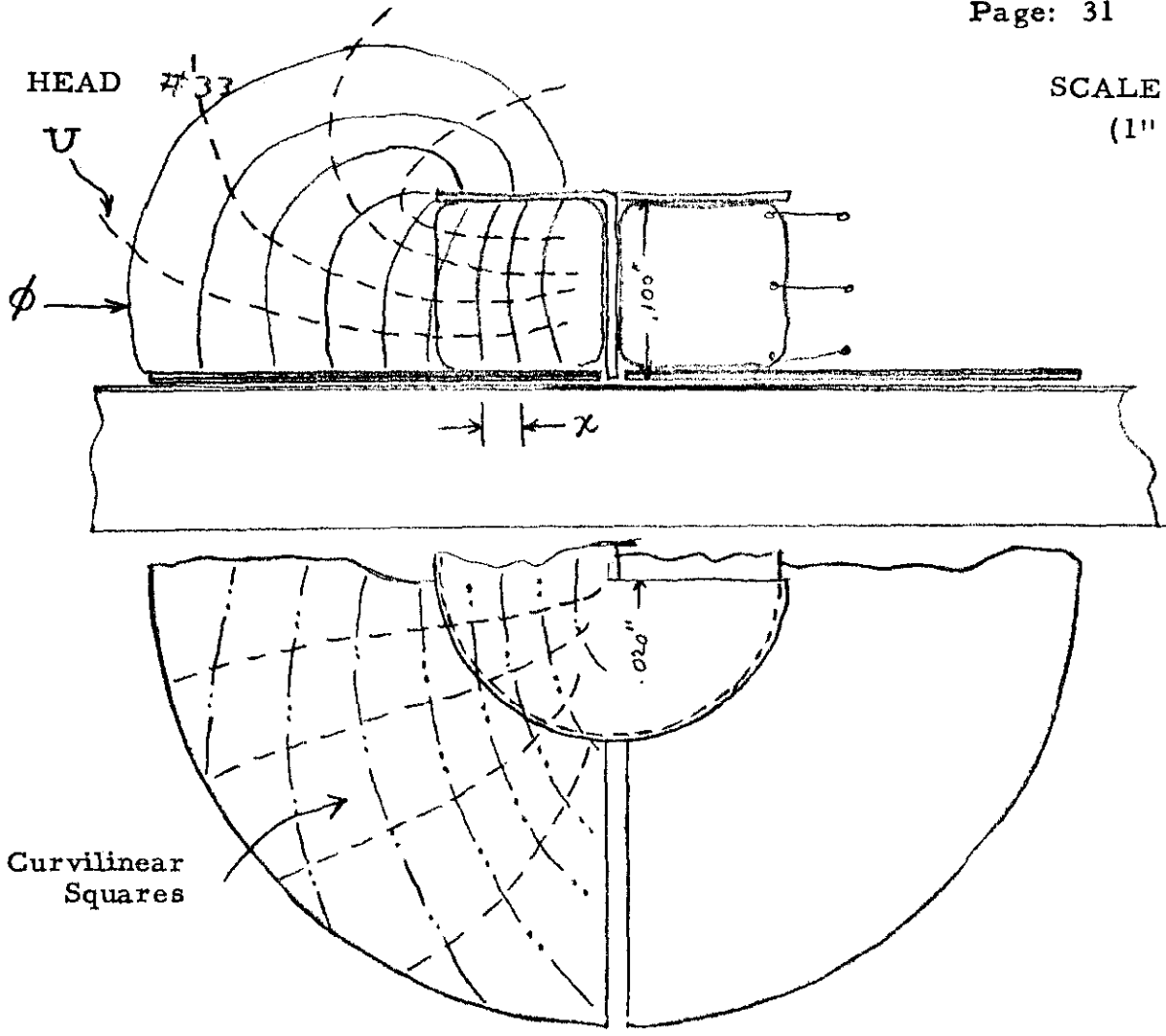


FIGURE 19 -- Approximate Flux Plot of Return Path for Head with Hat Type Shields.